The EMBO Journal (2011) 30, 4479–4488 | © 2011 European Molecular Biology Organization | Some Rights Reserved 0261-4189/11
www.embojournal.org

THE EMBO JOURNAL

EMBO open

Structural basis for cell surface patterning through NetrinG–NGL interactions

Elena Seiradake[1], Charlotte H Coles[1], Pavel V Perestenko[2], Karl Harlos[1], Robert Andrew Jeffrey McIlhinney[2], Alexandru Radu Aricescu[1,*] and Edith Yvonne Jones[1,*]

[1]Division of Structural Biology, CR-UK Receptor Structure Research Group, Wellcome Trust Centre for Human Genetics, University of Oxford, Oxford, UK and [2]MRC Anatomical Neuropharmacology Unit, University of Oxford, Oxford, UK

Brain wiring depends on cells making highly localized and selective connections through surface protein–protein interactions, including those between NetrinGs and NetrinG ligands (NGLs). The NetrinGs are members of the structurally uncharacterized netrin family. We present a comprehensive crystallographic analysis comprising NetrinG1–NGL1 and NetrinG2–NGL2 complexes, unliganded NetrinG2 and NGL3. Cognate NetrinG–NGL interactions depend on three specificity-conferring NetrinG loops, clasped tightly by matching NGL surfaces. We engineered these NGL surfaces to implant custom-made affinities for NetrinG1 and NetrinG2. In a cellular patterning assay, we demonstrate that NetrinG-binding selectivity can direct the sorting of a mixed population of NGLs into discrete cell surface subdomains. These results provide a molecular model for selectivity-based patterning in a neuronal recognition system, dysregulation of which is associated with severe neuropsychological disorders.

The EMBO Journal (2011) **30,** 4479–4488. doi:10.1038/emboj.2011.346; Published online 23 September 2011
Subject Categories: neuroscience; structural biology
Keywords: brain patterning; crystal structure; protein engineering; schizophrenia; synaptic adhesion

Introduction

The intricate choreography of cell populations required for embryonic morphogenesis and adult tissue homeostasis is directed by several distinct families of cell guidance cues. One major family, the netrins, interacts with diverse single pass cell surface receptors to mediate cell repulsion, attraction or adhesion in tissues, which include the nervous system, vasculature, lung, pancreas, mammary gland and muscle (Lai Wing Sun *et al*, 2011). The neuronal NetrinG1 and NetrinG2 are vertebrate specific and by binding their cognate NetrinG ligand (NGL) partners (Woo *et al*, 2009b), they promote thalamocortical axon outgrowth (Lin *et al*, 2003), induce and maintain excitatory synapse formation (Kim *et al*, 2006) and contribute to subdendritic segmentation in the hippocampus and cortex (Nishimura-Akiyoshi *et al*, 2007). Abnormal expression of NetrinGs is associated with behavioural phenotypes in mice (Zhang *et al*, 2008) and with schizophrenia, bipolar disease, temporal lobe epilepsy and Rett syndrome in humans (Aoki-Suzuki *et al*, 2005; Borg *et al*, 2005; Eastwood and Harrison, 2008; Ohtsuki *et al*, 2008; Pan *et al*, 2010). The third member of the NGL family, NGL3, does not bind netrins, instead regulating excitatory synapse formation through interaction with the type IIa receptor protein tyrosine phosphatases (Woo *et al*, 2009a; Kwon *et al*, 2010).

Sequence analysis predicts that the NetrinGs contain an extracellular N-terminal laminin-like domain (Lam) and, depending on the splice isoform, up to four epidermal-growth-factor-like (EGF) domains, and a C-terminal glycosylphosphatidylinisotol (GPI) anchor (Figure 1A) (Nakashiba *et al*, 2000, 2002; Yin *et al*, 2002). The N-terminal Lam domain is characteristic of the classic, secreted, netrin cell guidance factors and of the extracellular matrix laminin proteins (Supplementary Figures S1 and S2). NGLs are type I transmembrane (TM) proteins composed of nine leucine-rich repeats (*lrr*) forming the *lrr*-rich domain (LRR), an immunoglobulin-like domain (Ig), a highly glycosylated region (S), a TM helix and a cytoplasmic domain containing a PDZ-binding motif (Figure 1A). In the absence of any structural information for the NetrinGs, the NGLs or their recognition complexes, the determinants of binding selectivity and mode of interaction required for function have remained uncharacterized.

Results

Crystallographic analysis of NetrinG and NGL proteins

We present crystal structures of a NetrinG1$_{Lam-EGF1}$ + NGL1$_{LRR-Ig}$ complex, NetrinG2$_{Lam-EGF1}$, a NetrinG2$_{Lam-EGF1}$ + NGL2$_{LRR-Ig}$ complex and NGL3$_{LRR-Ig}$ determined at resolutions of 3.3, 2.2, 2.6 and 3.1 Å, respectively (Table I).

The core of the 269-residue NetrinG2 Lam domain comprises a β-sandwich with a 'jelly-roll' topology (Richardson, 1981) decorated by elaborate insertions including a helical region (Supplementary Figure S3; Figure 1B). The extended N-terminus forms a β-hairpin, which partially abuts the 58-residue C-terminal EGF1 domain. Extensive disulphide bonding in the Lam and EGF1 domains stabilize the intricate arrangement. The structure is most similar to that recently reported for the Lam domain of mouse LamininA5 (Hussain *et al*, 2011) (root mean square deviation, r.m.s.d., of 2.05 Å for 220 Cα atoms; Supplementary Figure S3).

The 391-residue NGL3$_{LRR-Ig}$ structure reveals an arrangement in which a C2-type Ig domain folds back onto the convex face of a horseshoe-shaped LRR domain (Figure 1C). In its domain composition, NGL3 resembles the neuronal Nogo-66 receptor-binding glycoprotein Lingo-1,

*Corresponding authors. AR Aricescu or EY Jones, Division of Structural Biology, CR-UK Receptor Structure Research Group, Wellcome Trust Centre for Human Genetics, University of Oxford, Roosevelt Drive, Oxford OX3 7BN, UK. Tel.: +44 186 528 7564; Fax: +44 186 528 7547; E-mail: radu@strubi.ox.ac.uk or Tel.: +44 186 528 7546; Fax: +44 186 528 7547; E-mail: yvonne@strubi.ox.ac.uk

Received: 13 July 2011; accepted: 25 August 2011; published online: 23 September 2011

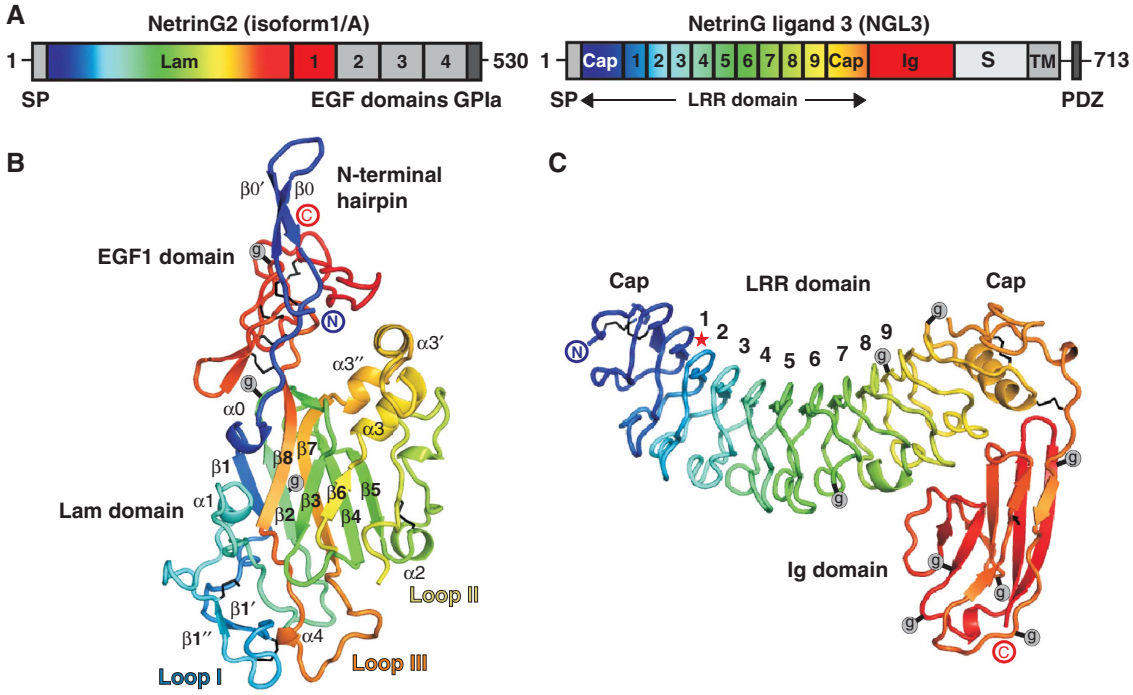

Figure 1 Crystal structures of unliganded $NetrinG2_{Lam-EGF1}$ and $NGL3_{LRR-Ig}$. (**A**) Domain organization of human NetrinG2 (isoform 1/A) and NGL3. Domain nomenclature as in main text. SP, signal peptide; GPIa, GPI anchor; Cap, N- and C-terminal Cap regions. (**B**) Ribbon diagram of $NetrinG2_{Lam-EGF1}$ (residues Y19–A345). Jelly-roll β-strands are labelled β1–β8. Three predicted N-linked glycosylation sites are marked with g enclosed in a grey circle. Black lines denote disulphide bridges. N- and C-termini are indicated (encircled N and C). (**C**) Ribbon diagram of $NGL3_{LRR-Ig}$ (residues S58–N454). *lrr*s are numbered 1–9. Q96, essential for binding of NGL3 to LAR (Kwon *et al*, 2010) is marked with a red star. Other labelling and colouring as for (**B**).

although the Lingo-1 LRR domain is larger by 3 *lrr*s (Mosyak *et al*, 2006) (Supplementary Figure S4). In common with all LRR domain proteins, the NGL3 *lrrs* are sandwiched by N-terminal and C-terminal cap structures.

Our complex structures show that the concave faces of the NGL1 and NGL2 LRR domains bind to their cognate NetrinGs through a complementarily shaped binding site on the Lam domain (Figure 2A and B), reminiscent of the hand-clasp mode described for other LRR-ligand binding interactions (Fan and Hendrickson, 2005; Bella *et al*, 2008). The total buried surface area (Krissinel and Henrick, 2007) in the complexes is $\sim$2410 Å^2 for $NetrinG1_{Lam-EGF1} + NGL1_{LRR-Ig}$ and $\sim$2080 Å^2 for $NetrinG2_{Lam-EGF1} + NGL2_{LRR-Ig}$. Multi-angle light scattering (MALS) measurements support a 1:1 stochiometry for both complexes (Supplementary Figure S5). In the crystal structures, the NetrinG and NGL C-termini point in opposite directions, an arrangement suitable for the *trans* interactions required for a functional role mediating binding events between neurons. The NGL-binding site on NetrinGs is essentially composed of the three long loops (I, II and III) located between strands β1–β2, β5–β6 and β7–β8, respectively (Figure 2A and B). In both complexes, loop I provides extensive interactions, primarily to conserved NGL residues. Loop II interacts via two non-conserved hydrogen bonds and hydrophobic interactions in the NetrinG1–NGL1 structure. In the NetrinG2–NGL2 complex, however, it provides little direct contact. Conversely, while NetrinG1 loop III provides only a few hydrophobic contacts to NGL1, NetrinG2 loop III binds to NGL2 with five hydrogen bonds plus additional hydrophobic interactions (Figure 2C–I). The conserved core of interactions contributed by loop I suggest an ancestral NetrinG–NGL interaction diversified with addition of homologue-specific interactions via loops II and III. Structural superposition of $NetrinG2_{Lam-EGF1}$ in its unliganded and NGL2-bound forms reveals an induced-fit binding mechanism affecting loop I (Cα r.m.s.d. 4.1 Å^2, contrasting with the overall r.m.s.d. of 1.6 Å^2) and loop II, which is disordered in the unbound form. Overlay of the two NGL-bound structures of NetrinG1 and NetrinG2 shows that conformational differences are, again, concentrated in the NGL-binding loops, consistent with a role as determinants of binding specificity (for loops I + II + III, the Cα r.m.s.d. is 3.3 Å^2, whereas the overall Cα r.m.s.d. is 1.8 Å^2). In contrast to the NetrinGs, the structures of $NGL1_{LRR-Ig}$ (complexed), $NGL2_{LRR-Ig}$ (complexed) and $NGL3_{LRR-Ig}$ (unliganded) are similar, suggesting that the structure of NGL_{LRR-Ig}s does not undergo major rearrangement upon ligand binding. There are, however, some subtle differences in the relative orientations of the Ig and LRR domains between the three NGL family members (Supplementary Figure S4). In combination, these data define a generic binding architecture for the NetrinG–NGL system, which comprises the docking of three flexible NetrinG loops onto a relatively rigid concave surface on NGL.

Wild-type NetrinG–NGL binding affinities

NetrinG1/NGL1 and NetrinG2/NGL2 have, in general, been observed to segregate to non-overlapping regions in the brain (Nakashiba *et al*, 2002; Yin *et al*, 2002; Kim *et al*, 2006; Nishimura-Akiyoshi *et al*, 2007). We refer to these cognate pairs as 'intra-class' binding partners and to interactions between members of different pairs as 'cross-class' binding. Using surface plasmon resonance (SPR) equilibrium

Table I Data collection and refinement statistics

	$NetrinG2_{Lam-EGF}$ (native)	$NetrinG2_{Lam-EGF}$ (selenomethionine)	$NGL3_{LRR}$	$NGL3_{LRR-Ig}$	$NetrinG1_{Lam-EGF}$ + $NGL1_{LRR\,Ig}$	$NetrinG2_{Lam-EGF}$ + $NGL2_{LRR-Ig}$
PDB accession code	3ZYG	—	3ZYN	3ZYO	3ZYJ	3ZYI
Data collection						
Space group	*C2*	*P1*	*C2*	*H32*	*F222*	*I222*
Cell dimensions						
a, *b*, *c* (Å)	111.5, 64.9, 120.1	64.4, 64.5, 120.9	157.1, 57.3, 100.4	131.3, 131.3, 174.9	184.4, 204.4, 288.1	75.4, 153.4, 158.7
α, β, γ (deg)	90, 103.1, 90	82.5, 75.1, 60.4	90, 117.8, 90	90, 90, 120	90, 90, 90	90, 90, 90
Resolution (Å)[a]	29.1–2.2 (2.4–2.2)	30–2.4 (2.5–2.4)	53–3.2 (3.28–3.2)	38.6–3.1 (3.27–3.1)	29.4–3.25 (3.4–3.25)	28.9–2.6 (2.7–2.6)
R_{meas} (%)[a]	17.3 (61.1)	23.1 (109)	20.6 (79.7)	13.6 (93.3)	20.6 (76.6)	9.2 (94.2)
$I/\sigma I$[a]	6.4 (2.35)	7.0 (1.8)	8.2 (2.2)	11.2 (2.6)	8.8 (1.5)	16.6 (2.1)
Completeness (%)[a]	98.9 (96.6)	95.5 (86.6)	99.6 (99.8)	99.9 (100)	91.3 (73.3)	98.7 (98.2)
Redundancy[a]	3.6 (3.4)	5.3 (4.6)	3.6 (3.6)	7.3 (7.4)	5.7 (2.7)	6.2 (6.3)
Refinement						
Resolution (Å)[a]	29.2–2.2 (2.26–2.2)	—	53–3.2 (3.28–3.2)	38.6–3.1 (3.18–3.1)	29.4–3.25 (3.33–3.25)	28.9–2.6 (2.7–2.6)
No. reflections	42 207 (2863)	—	12 344 (809)	10 223 (705)	39 039 (2266)	28 340 (2924)
R_{work}/R_{free}	0.246/0.291	—	0.217/0.268	0.229/0.269	0.257/0.268	0.246/0.287
No. atoms	5383	—	5027	3115	11 398	5450
Protein	5117	—	4999	3100	11 262	5411
Ligand/ion	58	—	28	15	136	39
Water	208	—	0	0	0	0
Average *B*-factors						
Protein	25.7	—	42.2	103	102	58.7
Ligand/ion	27.2	—	54.8	122.7	105	80.2
Water	21.4	—	—	—	—	—
R.m.s.d.						
Bond lengths (Å)	0.01	—	0.006	0.005	0.007	0.008
Bond angles (deg)	1.11	—	0.986	0.857	0.93	1.00

[a]Values in parentheses are for the highest-resolution shell.

experiments, we measured intra-class affinities of 7.9 nM (NetrinG1–NGL1) and 7.3 nM (NetrinG2–NGL2), values lying within the range reported previously (Lin *et al*, 2003; Nishimura-Akiyoshi *et al*, 2007; Zhang *et al*, 2008). We found that the introduction of an N-linked glycosylation site in the NetrinG-binding site on NGL1 (A205T) and NGL2 (G204T) abolished NetrinG–NGL binding, in agreement with the binding interface revealed by the crystal structures (Figure 3). Interestingly, we were able to measure previously undetected cross-class binding affinities, albeit in the low micromolar range: 4.9 μM (NetrinG1–NGL2) and 2.0 μM (NetrinG2–NGL1) (Figure 4; Supplementary Figure S6). It remains to be established whether these low affinity interactions play any functional role *in vivo*. Consistent with previous reports (Kim *et al*, 2006), we find that the affinity between NGL3 and either NetrinG is very weak ($K_d > 100$ μM).

Engineering of protein binding affinities

To dissect the precise determinants of NGL specificity, we introduced point mutations in the NetrinG-binding surface of NGL1, which transplanted the corresponding NGL2 surface (Figure 3; Supplementary Figure S7). A swap of nine non-conserved residues in the loop I binding region (NGL1-r1 mutant), does not result in a major increase of affinity to NetrinG2 (<2-fold), although binding to NetrinG1 is decreased >10-fold (Figure 4; Supplementary Figure S8). Thus, as we hypothesised based on the structural results, the interactions provided by loop I are not the main determinants for binding specificity. In contrast, when we transplanted the NGL2 surfaces corresponding to the binding regions for loop II (NGL1-r2 mutant, switching four residues) or loop III (NGL1-r3 mutant, switching seven residues), we observed a reversal of the wild-type (WT) binding preference to favour cross-class binding (Figure 4; Supplementary Figure S8). This is consistent with the interactions mediated by regions 2 and 3 providing the major components of binding specificity. For all three individual NGL1-r1, -r2 and -r3 mutants, the binding selectivity is decreased compared with WT NGL1, consistent with these mutant binding surfaces comprising a patchwork of NGL1 and NGL2 elements. A combined transplant of all three NGL2 regions into NGL1 (NGL1-r123 mutant), or conversely, of NGL1 regions into NGL2 (NGL2-r123 mutant), results in a complete switch in NetrinG specificity (Figure 4; Supplementary Figure S8).

As expected based on the crystal structures of the complexes, we were able to impair binding in SPR assays by introducing an N-linked glycosylation site in the NGL-binding site of NetrinG1 or NetrinG2 loop I (Supplementary Figure S8). We then attempted to manipulate specificities in the NetrinG1 and NetrinG2 proteins by swapping one, two or all three main NGL-binding loops. This panel of mutants displays a plethora of NGL-binding properties, summarized and discussed in Supplementary Figure S8. Thus, while the rigid scaffold of the NGL LRR domain can be subdivided into a mosaic of essentially discrete NetrinG-binding regions, the flexible loops of the NetrinGs cannot be treated as stand-alone structural elements.

NetrinG-binding controls cell surface NGL patterns

Analyses of NetrinG-deficient mice have demonstrated that NetrinG1 and NetrinG2, expressed on different sets of axonal projections, are essential for localizing NGL1 and NGL2, co-expressed in the receiving dendrite, to distinct dendritic subdomains in hippocampal or cortical neurons

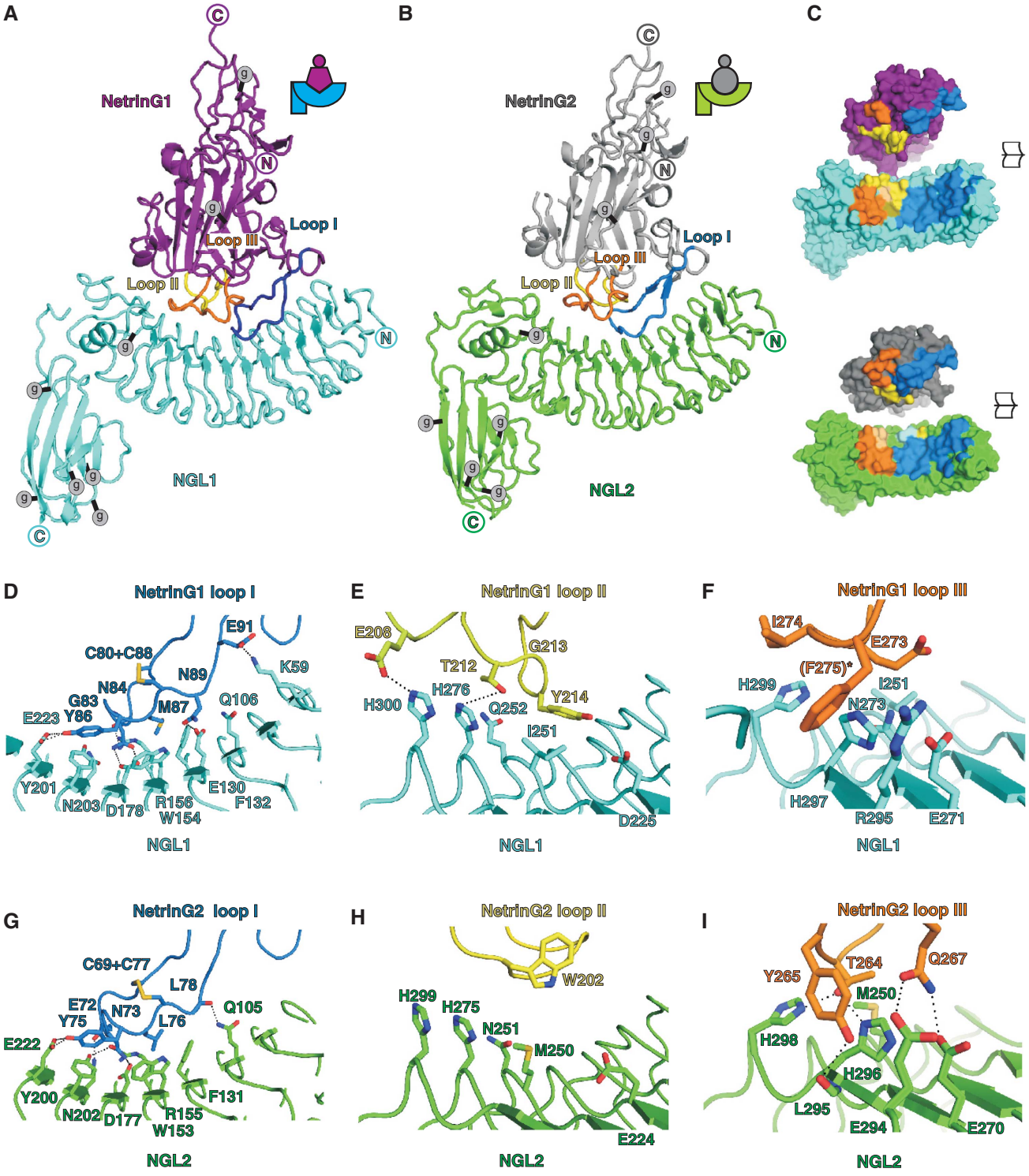

Figure 2 Similar surfaces with distinct binding properties mediate NetrinG–NGL interactions. (**A**) Ribbon diagram of NetrinG1$_{\text{Lam–EGF1}}$ (purple) in complex with NGL1$_{\text{LRR–Ig}}$ (cyan). Main NGL1-binding loops are coloured separately. Predicted N-linked glycosylation sites are marked with g enclosed in a grey circle. (**B**) Ribbon diagram of NetrinG2$_{\text{Lam–EGF1}}$ (grey) in complex with NGL2$_{\text{LRR–Ig}}$ (green). Predicted N-linked glycosylation sites and NGL2-binding loops are indicated. (**C**) Open surface views showing NetrinG1–NGL1 and NetrinG2–NGL2 interfaces. NGL1 (cyan) and NGL2 (green) residues in the binding interface are coloured according to the NetrinG loop they contact: blue (loop I), yellow (loop II), orange (loop III), mustard (loop I and loop III), light orange (loop II and loop III), light blue (loop I and loop II). (**D–I**) Views of selected residues in the NetrinG1–NGL1 and NetrinG2–NGL2 interfaces. Hydrogen bonds are shown as dotted lines. Colours as for (**A**, **B**). The side chain of NetrinG1 F275, labelled with an asterisk, is depicted for completeness although poorly defined in the electron density (**F**). The backbone carbonyl oxygen of NetrinG2 L295, but not the side chain, is shown in stick representation (**I**).

(Nishimura-Akiyoshi *et al*, 2007). We developed an assay to test the ability of NetrinGs to induce and maintain such compartmentalization of NGLs at the surface of HEK293T cells. Cells over-expressing either GPI-anchored NetrinG1 or NetrinG2 were plated alongside cells co-expressing full-length (TM) NGL1 and NGL2. We found that, indeed, contact

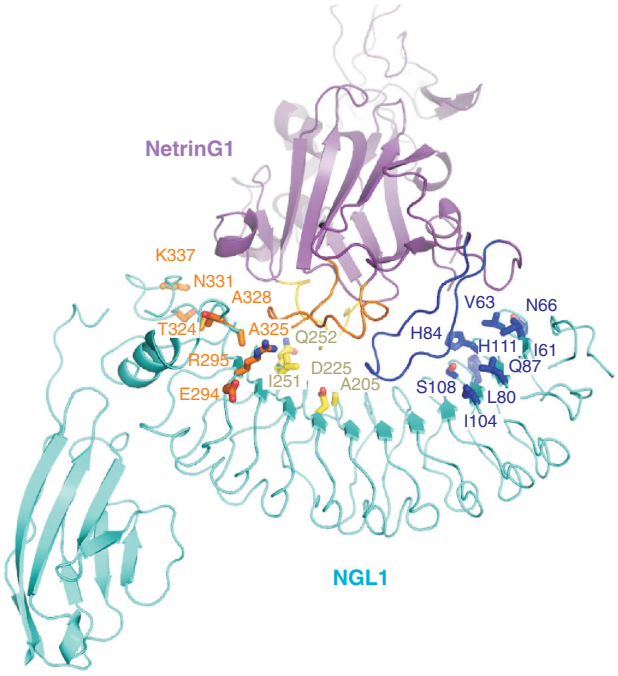

Figure 3 Non-conserved residues in the concave LRR surfaces of NGL1 and NGL2 were swapped to create proteins with modified binding specificities. Differences between NGL1 and NGL2 are concentrated at the N-terminal and C-terminal regions of the binding surface, with only few variations found in the central region. In the NGL1-r1 mutant, non-conserved residues in the vicinity of the NetrinG loop I binding site were swapped (shown in blue, stick representation). These include NGL1 residues I61, V63, N66, L80, H84, Q87, I104, S108 and H111, equivalent to NGL2 residues V60, T62, G65, Y79, M83, N86, V103, G107 and S110. In NGL1-r2, residues around the loop II binding site were swapped (shown in yellow). These include NGL1 residues A205, D225, I251 and Q252, equivalent to NGL2 residues G204, E224, M250 and N251. In NGL1-r3, residues including those in the loop III binding site were swapped (NGL1 residues E294, R295, T324, A325, A328, N331 and K337, equivalent to NGL2 residues V293, E294, S323, T324, G327, H330 and R336, shown in orange). In NGL1-r123, all non-conserved residues in the binding interface were swapped. *Vice versa*, in NGL2-r123, the equivalent residues were swapped to match those found in NGL1. The NetrinG-binding specificities of these mutants were analysed using SPR (Figure 4; Supplementary Figure S8).

with NetrinG1- or NetrinG2-expressing cells led to the exclusive targeting of NGL1 or NGL2 to the cell–cell interface, respectively (Figure 5A and B; Supplementary Movie). We then exploited our findings on the determinants of NetrinG-binding specificity to switch the NetrinG-binding properties of NGL1 in live cells. We co-expressed full-length NGL1-r123 with NGL2, and found that both proteins were targeted to cell–cell interfaces with NetrinG2-, but not NetrinG1-, presenting cells (Figure 5C and D). Thus, the low affinity interactions measured for cross-class binding are not enough to build up intra-cellular NGL patterns efficiently. Further, the specificity determinants revealed by combined structural and biophysical analyses are sufficient (even when transplanted into the cross-class NGL) to control molecular sorting in a cellular context through *trans* recognition events. Thus, the binding affinity and selectivity conferred on the NetrinG–NGL interaction by the specificity determinants we have identified provide the properties necessary to generate and maintain the reported compartmentalization of NGL1 and NGL2 to distinct dendritic subdomains (Figure 6), as proposed for a 'lock-in' type model (Nishimura-Akiyoshi *et al*, 2007).

Discussion

Multiple mechanisms are required to direct brain development, controlling patterning and neuronal circuit formation at the laminar, cellular, subcellular and synaptic levels (Sanes and Yamagata, 2009; Williams *et al*, 2010; Tessier-Lavigne and Kolodkin, 2011). NetrinG–NGL interactions have been implicated in functions at each of these levels (Lin *et al*, 2003; Kim *et al*, 2006; Nishimura-Akiyoshi *et al*, 2007), culminating in *trans*-synaptic adhesion and synaptogenesis (Kim *et al*, 2006). Our results reveal the hand-clasp architecture and define the specificity-conferring elements of the NetrinG–NGL adhesive interaction. The selectivity of adhesive interactions has been shown to drive sorting at the cellular level, for example, cadherin-mediated motor neuron segregation (Patel *et al*, 2006) and Dscam isoform-coded dendritic self-avoidance (Meijers *et al*, 2007; Sawaya *et al*, 2008). However, the molecular systems that drive subcellular compartmentalization events are as yet poorly resolved. Molecules known to perform this role include members of the Ig superfamily (Ango *et al*, 2004) and semaphorins plus their cognate plexin receptors (Suto *et al*, 2007). In such cases, pre-established patterns of molecules on receiving dendrites determine the subcellular localization of synapses with in-coming axons (Ango *et al*, 2004; Suto *et al*, 2007). In contrast, the NetrinG–NGL system exemplifies how subcellular molecular patterns, that is, NGL1-rich versus NGL2-rich regions on dendrites, can be induced by pre-synaptic components, the layer-specific NetrinG cues. Our results on NetrinG–NGL provide a paradigm whereby the discrimination generated by adhesive binding affinity drives the sorting of a mixed population of molecules into discrete cell surface subdomains.

Materials and methods

Cloning and vectors

We cloned hexahistidine-tagged constructs of human NetrinG1$_{Lam-EGF1/4}$ (GenBank: BC030220.1, residues M1-H418, corresponding to domains Lam + EGF1 + EGF4, thus equalling isoform 1 minus the GPI-anchor region), human NetrinG2$_{Lam-EGF1}$ (GenBank: BC013770.1, residues M1-A345, corresponding to domains Lam + EGF1), human NGL1$_{LRR-Ig}$ (GenBank: BC041374.2, residues A44-T444, corresponding to domains LRR + Ig), human NGL2$_{LRR-Ig}$ (GenBank: NP_071426.1, residues M1-A444, corresponding to domains LRR + Ig), mouse NGL3$_{LRR}$ and NGL3$_{LRR-Ig}$ (GenBank: BC060263, residues M1-A365, corresponding to the LRR domain and residues M1-V455, corresponding to domains LRR + Ig) into the multiple cloning site of pHLsec or pHL-Avitag3 (Aricescu *et al*, 2006) using standard PCR methods and the restriction sites *Eco*RI and *Kpn*I (NetrinG1, NetrinG2, NGL2, NGL3) or *Age*I and *Kpn*I (NGL1). The NetrinG1 construct used for crystallization harbours two threonine to alanine mutations (T350A + T353A) to avoid predicted O-linked glycosylation.

We generated 23 mutant and hybrid NGL and NetrinG proteins, including the following:

(a) Knockout constructs (KO) harbouring N-linked glycosylation sites in the NetrinG–NGL binding interfaces designed to disrupt binding (NetrinG1 P85A + Y86T, NetrinG2 P74A + Y75T, NGL1 A205T, NGL2 G204T).

(b) NetrinG1$_{Lam-EGF1/4}$ and NetrinG2$_{Lam-EGF1}$ proteins where one or more NGL-binding loops are swapped. To swap loop I, we exchanged residues 81–90 (AMGNPYMCNN) in NetrinG1 and residues 70–79 (SHENPYLCSN) in NetrinG2. For loop II, we swapped residues 212–220 (TGYTTNSKI) in NetrinG1 and residues 201–209 (RWAGSKKEKH) in NetrinG2. For loop III, we

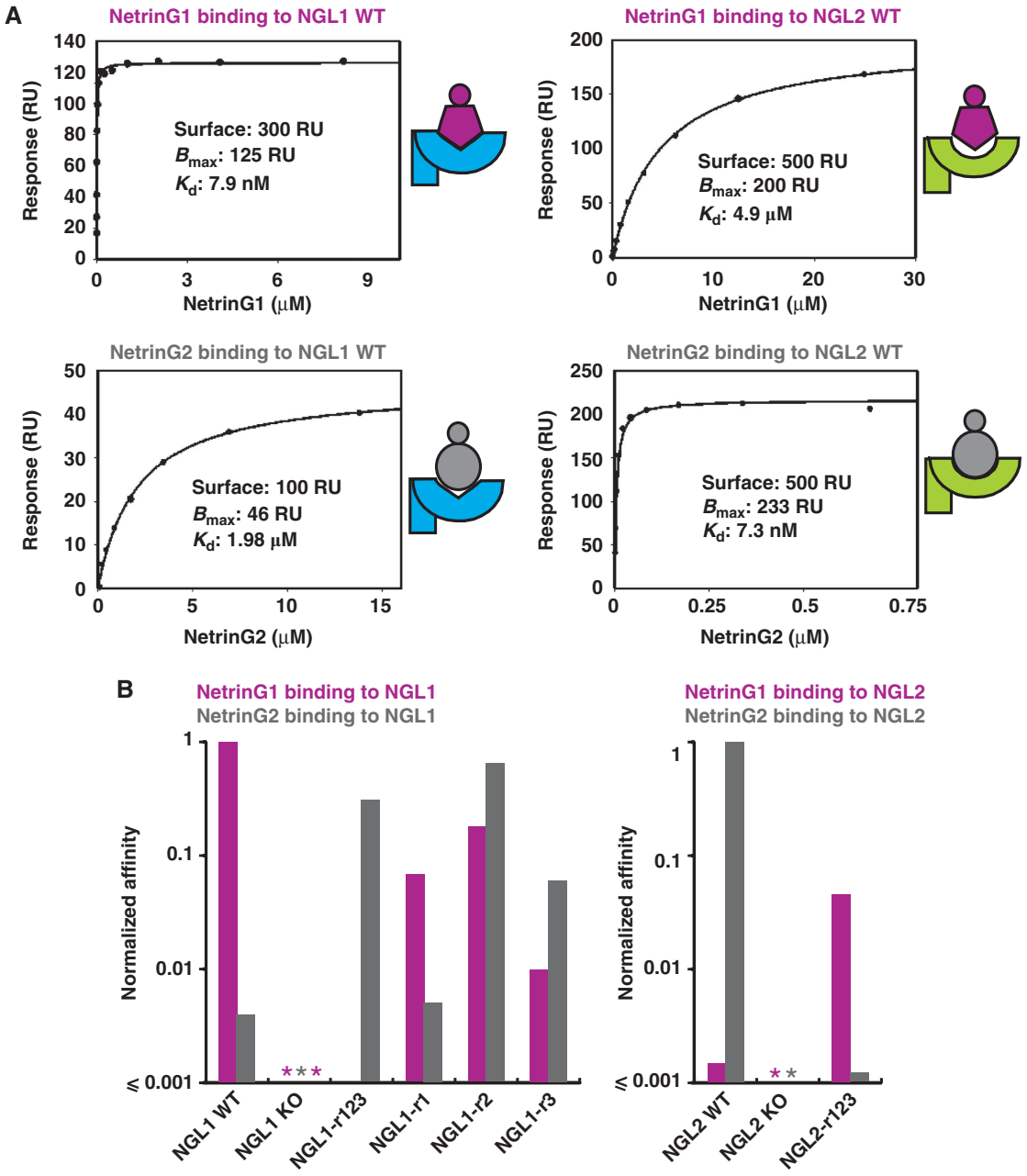

Figure 4 Manipulation of NetrinG–NGL recognition by structure-guided grafting of specificity. (**A**) SPR experiments for the interaction of WT NetrinG1$_{Lam-EGF1/4}$ and NetrinG2$_{Lam-EGF1}$ with WT NGL1/2$_{LRR-Ig}$ reveals intra-class binding K_ds in the low nanomolar range and cross-class binding K_ds in the low micromolar range. (**B**) The affinities depicted were normalized using the K_d value for WT intra-class binding. Binding to NGL constructs by NetrinG1 is shown in purple, binding by NetrinG2 is shown in grey. Introduction of an N-linked glycosylation site in the interface results in the loss of NetrinG binding (NGL1 KO and NGL2 KO), as indicated with an asterisk. NetrinG1$_{Lam-EGF1/4}$ contains an extra EGF domain compared with NetrinG2$_{Lam-EGF1}$. Addition of this domain does not affect the affinity of NetrinG1 to NGL1$_{LRR-Ig}$ or NGL2$_{LRR-Ig}$ (unpublished observation).

exchanged NetrinG1 residues 271–279 (VGEIFVDEL) and NetrinG2 residues 261–269 (LGGTYVQRE).

(c) NGL$_{LRR-Ig}$ constructs, in which one or more surface regions within the LRR concave face were exchanged between NGL1 and NGL2. The residues manipulated are depicted in Figure 3.

Production of NetrinG and NGL proteins

We expressed NetrinG, NGL1 and NGL2 ectodomain constructs transiently in GnTI-deficient HEK293S cells (Aricescu *et al*, 2006; Chang *et al*, 2007), then dialysed the cell medium against phosphate-buffered saline (PBS), loaded it onto a Ni-containing affinity column (His-Trap, GE Healthcare), washed with 20 mM Tris pH 7.5, 300 mM NaCl, 40 mM imidazole and eluted the protein with 20 mM Tris pH 7.5, 300 mM NaCl, 500 mM imidazole. For crystallization, we incubated proteins overnight at room temperature with 1:20 recombinant endoglycosidase F1 (Grueninger-Leitch *et al*, 1996; Chang *et al*, 2007). To remove the endoglycosidase, we diluted the protein 1:10 in 20 mM Tris pH 7.5, 300 mM NaCl, re-loaded it on a Ni-containing column, washed and re-eluted. The eluted protein was concentrated and loaded on a Superdex 200 column (GE Healthcare) previously equilibrated with 200 mM NaCl and 20 mM Tris pH 7.5. We expressed NGL3 constructs similarly, but after two-fold dilution in PBS pH 7.5, we loaded cell medium directly onto a Ni affinity column. We washed the column with PBS pH 7.5 containing 30 mM imidazole and eluted the protein by increasing the imidazole concentration to 500 mM. After 1:20

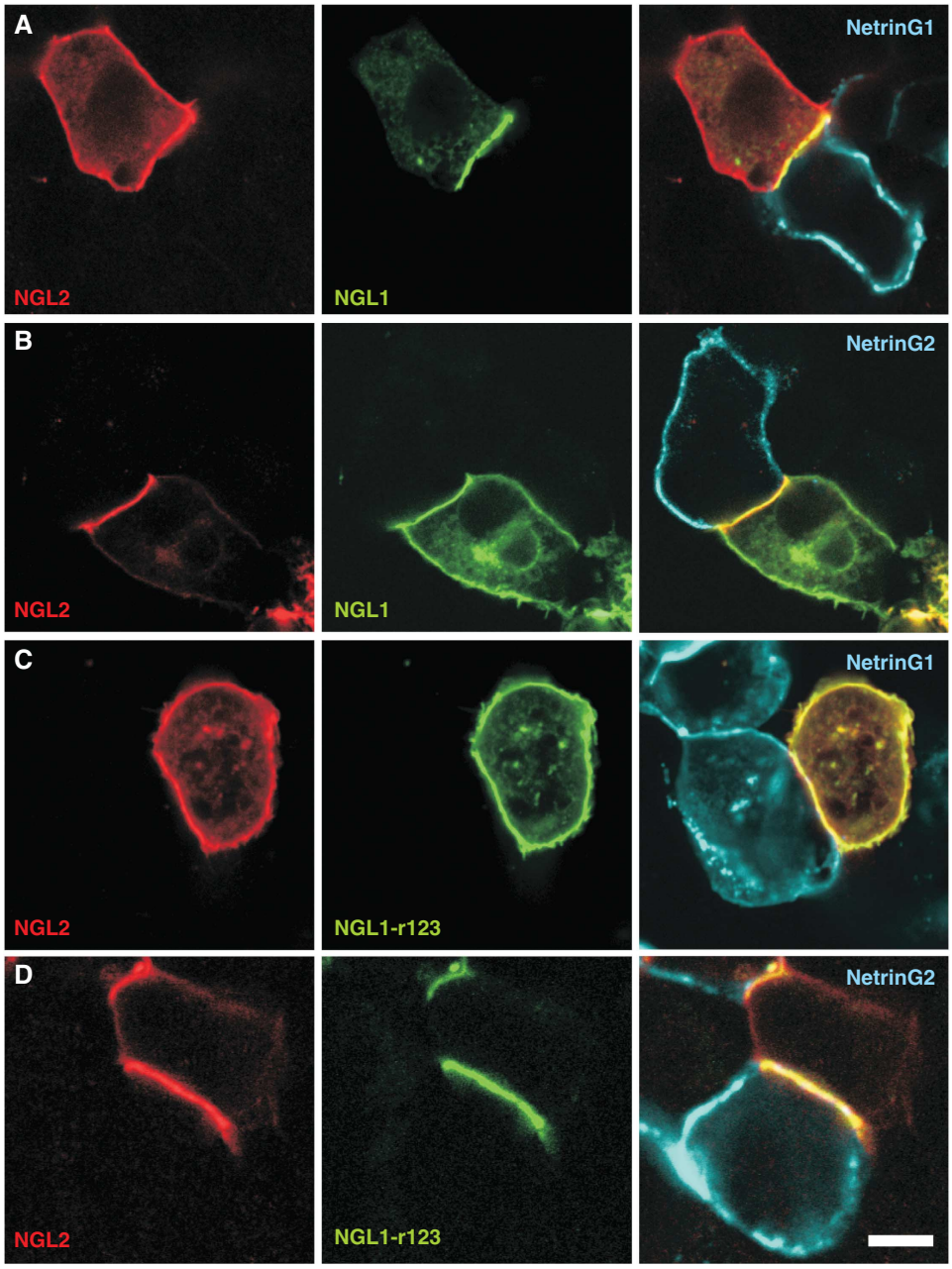

Figure 5 NetrinG-binding properties determine subcellular NGL localization. HEK293T cells co-expressing full-length TM NGL1-mVenus (green) and NGL2-mCherry (red) were grown alongside cells expressing GPI-anchored NetrinGs (blue). (**A**) Predominantly NGL1, and not NGL2, localizes to interfaces with NetrinG1-expressing cells. (**B**) NGL2 localizes to interfaces with NetrinG2-expressing cells. (**C**) NGL2 and NGL1-r123 (full-length) have less propensity to localize at cell–cell contacts with NetrinG1-presenting cells. (**D**) Both NGL2 and NGL1-r123 localize at interfaces with NetrinG2-presenting cells. The scale bar corresponds to 10 μm (**A**), 9.3 μm (**B**), 8.6 μm (**C**), 6 μm (**D**).

endoglycosidase F1 treatment for 3 h at 37°C, we exchanged the buffer to 50 mM HEPES, 50 mM NaCl pH 7.5, loaded the protein onto a heparin affinity column (HiTrap heparin HP, GE Healthcare) and eluted it with a sodium chloride gradient. We further purified NGL3 proteins by size-exclusion chromatography (Superdex 75, GE Healthcare) in 10 mM HEPES, 150 mM NaCl pH 7.5.

We produced complexes of NetrinG and NGL by mixing cognate binding partners in a 1:1 molar ratio prior to injection on a Superdex 200 column. We pooled fractions from the main protein peak, supplemented the samples with 100 mM non-detergent sulfobetaine 256 (Hampton) and concentrated for crystallization. Final protein concentrations were 5.3 mg/ml ($NetrinG2_{Lam-EGF1}$), 4.1 mg/ml ($NetrinG1_{Lam-EGF1/4} + NGL1_{LRR-Ig}$), 7.5 mg/ml ($NetrinG2_{Lam-EGF1} + NGL2_{LRR-Ig}$), 1.5 mg/ml ($NGL3_{LRR}$) and 4 mg/ml ($NGL3_{LRR-Ig}$). We expressed selenomethionine-labelled $NetrinG2_{Lam-EGF1}$ according to previously published protocols (Aricescu *et al*, 2006) and carried out purification and crystallization as for the native protein.

Protein crystallization

Crystals grew in 100 nl + 100 nl sitting nanodrops by the vapour diffusion method at 20°C (Walter *et al*, 2005). The crystallization conditions were 20% MME550, 0.1 M NaCl, 0.1 M bicine pH 9 ($NetrinG2_{Lam-EGF1}$), 2% PEG 400, 2 M ammonium sulphate, 0.1 M HEPES pH 7.5 + additive = PEG400 ($NetrinG1_{Lam-EGF1/4} + NGL1_{LRR-Ig}$), 50% v/v 2-methyl-2,4-pentanediol, 0.2 M ammonium di-hydrogen phosphate, 0.1 M Tris pH 8.5 ($NetrinG2_{Lam-EGF1} + NGL2_{LRR-Ig}$), 0.8 M succinic acid, pH 7.0 ($NGL3_{LRR}$) and 0.1 M NaH_2PO_4, 0.1 M KH_2PO_4, 2 M NaCl, 0.1 M MES pH 6.5 ($NGL3_{LRR-Ig}$). We collected X-ray diffraction images at the Diamond

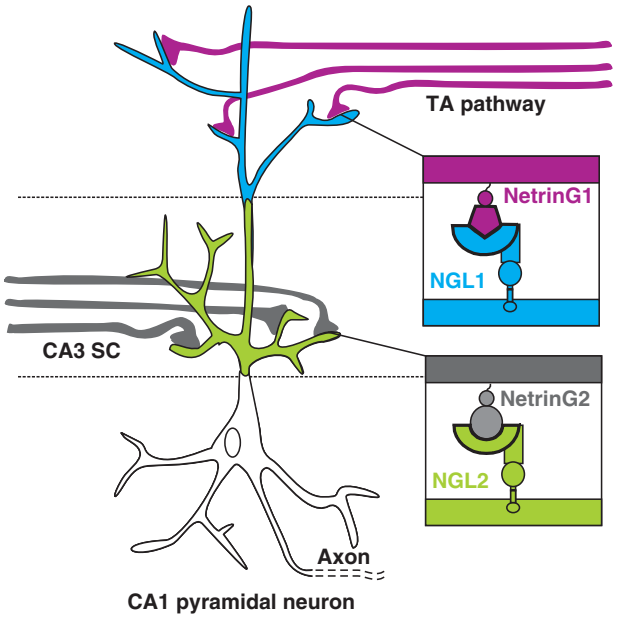

Figure 6 Schematic illustrating the structurally encoded NetrinG–NGL binding selectivity driving subcellular NGL localization in hippocampal CA1 pyramidal cells. CA1 dendrites receive inputs from apposing layers enriched in either NetrinG1-expressing axons (from the temporoammonic pathway, TA) or NetrinG2-expressing axons (Schaffer collaterals, SC, coming from the CA3 hippocampal region). These inputs localize NGL1 and NGL2 to distinct subdendritic regions via intra-class NGL–NetrinG interaction (Nishimura-Akiyoshi *et al*, 2007; Woo *et al*, 2009b).

Light Source beamlines I02, I03 and I04 and processed the data using XDS (Kabsch, 1993), HKL2000 (Otwinowski and Minor, 1997), xia2 (Winter, 2010) and programs from the CCP4 suite (Collaborative Computational Project 4, 1994).

Structure solution and model refinement

We used a fragment containing nine *lrr* repeats of the Lingo-1 crystal structure (PDB accession number 2ID5), with side chains trimmed to Cβ atoms using Chainsaw (Collaborative Computational Project 4, 1994), as the initial search model for molecular replacement with the 3.2 Å $NGL3_{LRR}$ data set in PHASER (McCoy *et al*, 2007). The resultant model consists of two copies in the asymmetric unit. We used Phenix Autobuild (Terwilliger *et al*, 2008) and manual adjustments in Coot (Emsley and Cowtan, 2004) to rebuild the core of the LRR domain and used the resultant model together with an NMR structure of the Ig domain of human NGL3 (PDB accession number 2DL9), for molecular replacement with the 3.1 Å $NGL3_{LRR-Ig}$ data set in PHASER (McCoy *et al*, 2007). Using Phenix Autobuild (Terwilliger *et al*, 2008) and parallel refinement of both $NGL3_{LRR}$ and $NGL3_{LRR-Ig}$ structures with Phenix (Adams *et al*, 2010), Buster (Blanc *et al*, 2004) and Refmac (Murshudov *et al*, 1997) resulted in final models containing residues 57–366 and 55–366 for molecules A and B of $NGL3_{LRR}$ and 58–454 (with the exception of two disordered loops, 68–69 and 335–338) of $NGL3_{LRR-Ig}$.

We derived initial phases for the $NetrinG2_{Lam-EGF1}/NGL2_{LRR-Ig}$ complex data (space group *I222*) from molecular replacement using the model of $NGL3_{LRR-Ig}$ and that of human HSPB11 (PDB accession code 1TVG) (McCoy *et al*, 2007; Ramelot *et al*, 2009), which we predicted, using Fugue (Shi *et al*, 2001), to be structurally related to the NetrinG2 Lam domain. The resulting electron density map allowed manual building (Emsley and Cowtan, 2004) and refinement (Blanc *et al*, 2004) of an initial $NetrinG2_{Lam-EGF1}$ model, which we used as molecular replacement model with the selenomethionine derivative data for unliganded $NetrinG2_{Lam-EGF1}$ in Phaser (McCoy *et al*, 2007). This selenomethionine data set was analysed using space group *P1* and displayed translational non-crystallographic symmetry (Patterson off-origin peak = 64% of origin). The molecular replacement solution was used to determine selenium positions with PHASER (McCoy *et al*, 2007) and the resulting maps and selenium substructure were then used to manually improve (Emsley and Cowtan, 2004) the Netrin $G2_{Lam-EGF1}$ model. We took the resultant model for molecular replacement with the high-resolution native data set of Netrin-$G2_{Lam-EGF1}$ (indexed according to the space group *C2*, with Patterson off-origin peak = 32% of origin), fully built (Emsley and Cowtan, 2004) and refined (Blanc *et al*, 2004) it, and then fed it back into the $NetrinG2_{Lam-EGF1}/NGL2_{LRR-Ig}$ complex structure for refinement (Blanc *et al*, 2004) of the complex. The resulting model served to phase the $NetrinG1/NGL1_{LRR-Ig}$ data (space group *F222*) by molecular replacement (McCoy *et al*, 2007). We fully refined all models using autoBuster (Blanc *et al*, 2004). In contrast to the $NetrinG2_{Lam-EGF1}$ construct, the $NetrinG1_{Lam-EGF1/4}$ construct comprises two EGF domains. In the crystal, this second EGF domain points towards a solvent channel. Although there is space to accommodate the second EGF domain in the lattice, there was no interpretable electron density, suggesting that it is flexibly connected to the rest of the protein and adopts multiple conformations in the crystal. We therefore refer to the crystal structure resulting from the $NetrinG1_{Lam-EGF1/4}$ construct as $NetrinG1_{Lam-EGF1}$. Interestingly, constructs lacking this second EGF domain failed to crystallize in our hands, further supporting the presence of full-length $NetrinG1_{Lam-EGF1/4}$ in the crystal. An N-linked sugar that was not cleaved during the deglycosylation process contributes to crystal packing and consequently has well-ordered electron density for one of the two $NetrinG1_{Lam-EGF1}$ copies in the asymmetric unit. We used Molprobity (Davis *et al*, 2007) to assess the quality of all protein models. Diffraction data and refinement details are summarized in Table I. We used Coot to superpose molecules for the calculation of root mean square deviation (r.m.s.d.) between Cα atoms. To calculate r.m.s.d. values for NetrinG loops I–III, we defined NetrinG1 residues 74–82 and NetrinG2 residues 63–82 as loop I, NetrinG1 residues 209–219 and NetrinG2 residues 198–209 as loop II and NetrinG1 residues 270–280 and NetrinG2 residues 260–270 as loop III. The shape correlation statistic (S_c), a parameter that describes the shape complementarity of two protein surfaces (Lawrence and Colman, 1993), is 0.62 for the $NetrinG1_{Lam-EGF1} + NGL1_{LRR-Ig}$ complex and 0.69 for $NetrinG2_{Lam-EGF1} + NGL2_{LRR-Ig}$, consistent with tight interactions.

Multiangle light scattering

We purified protein samples by size-exclusion chromatography and concentrated to ~0.5–1 mg/ml. Separation for MALS was achieved using an analytical Superdex S200 10/30 column (GE Healthcare) and the eluate was passed through online static light scattering (DAWN HELEOS II, Wyatt Technology, Santa Barbara, CA), differential refractive index (Optilab rEX, Wyatt Technology) and Agilent 1200 UV (Agilent Technologies) detectors. We analysed data using the ASTRA software package (Wyatt Technology).

SPR experiments

Mutant and WT proteins were tested in SPR equilibrium experiments where the native membrane topology was mimicked by coupling of proteins to a streptavidin-coated chip via a C-terminal-linked biotin label. We used a Biacore T100 machine (GE Healthcare) at 25°C in a running buffer comprising 10 mM HEPES, pH 7.5, 150 mM NaCl, 0.005% (v/v) polysorbate 20. All proteins underwent size-exclusion chromatography in running buffer before SPR experiments. To mimic the native membrane insertion topology, we biotinylated proteins enzymatically at an engineered C-terminal tag (Aricescu *et al*, 2006) and attached them via the biotin label to streptavidin that was covalently coupled to the Biacore chip surface (O'Callaghan *et al*, 1999). The signal from experimental flow cells was corrected by subtraction of a blank and reference signal from a mock-coupled flow cell in Scrubber2 (BioLogic). In all experiments analysed, the experimental trace returned to baseline after a regeneration step with 2 M $MgCl_2$. K_d and maximum analyte binding (B_{max}) values were obtained by non-linear curve fitting of a 1:1 Langmuir interaction model (bound = $B_{max}/(K_d + C)$, where C is the analyte concentration calculated as monomer). The NetrinG1 construct used for crystallization harbours two threonine to alanine mutations (T350A + T353A) to avoid predicted O-linked glycosylation. As expected from their distance to the NGL-binding site, we found these mutations do not affect the affinity to NGL1 in SPR experiments. Compared with NetrinG2, the NetrinG1 construct we used in crystallization and SPR experiments

contains an additional EGF domain. As expected from the crystal structures, we found that removal of EGF4 does not affect the NetrinG1–NGL1 binding affinity (unpublished observation).

Cell surface patterning assay

Full-length human NGL1 (WT or harbouring the NGL1-r123 mutations) and NGL2 were fused to C-terminal mVenus-His or mCherry-His tags by subcloning into the appropriate pHLsec vector backbone. Full-length NetrinG1 isoform 1 (including the GPI anchor) or NetrinG2$_{Lam-EGF1}$ fused to residues C502–R530 (equivalent to the C-terminal NetrinG2 GPI-anchor sequence) were subcloned into pHLsec without further tags. We grew HEK293T cells in Dulbecco's modified Eagle's Medium (DMEM high glucose; Sigma) supplemented with L-glutamine, non-essential amino acids (Gibco) and 10% (v/v) fetal calf serum (FCS; Sigma) and transfected plasmid DNA (full-length NGL1 + NGL2, NetrinG1 isoform 1 or NetrinG2 GPI-fusion) using lipofectamine 2000 following the recommended protocol (Invitrogen). Final concentrations were 2 μg plasmid DNA per ml, 5 μl lipofectamine per ml and 1.5% (v/v) FCS. After 4–5 h, we replaced the transfection mix with original growth medium, re-suspended the cells and plated these on poly-L-lysine-coated glass bottom culture plates (MatTek). To observe *trans* interactions of different constructs, we mixed separately transfected cells at this stage. After 4% paraformaldehyde fixation for 10 min, to visualize NetrinG-expressing cells, the samples were stained with PBS containing 10 μg/ml His-tagged NGL1$_{LRR-Ig}$ or NGL2$_{LRR-Ig}$, 5 μg/ml mouse anti-Penta-His (Qiagen) and 6 μg/ml Alexa647-conjugated anti-mouse (Invitrogen). We took multicoloured fluorescent images (1024 × 1024 pixel, 4 scans per frame, sequential scanning) with an LSM510 inverted confocal microscope system and Plan-NEOFLUAR ×40/1.3 oil DIC immersion lens (Carl Zeiss Ltd., Welwyn Garden City, UK), excitation 488 nm and emission 500–550 nm by-pass filter, excitation 543 nm and emission 565–615 nm by-pass filter or excitation 633 nm and emission 650 nm long-pass filter, optical slice 0.1 μm.

Supplementary data

Supplementary data are available at *The EMBO Journal* Online (http://www.embojournal.org).

Acknowledgements

We thank Y Zhao and W Lu for protein expression; B Janssen and T Malinauskas for assistance with SPR experiments; M Jones and TS Walter for technical support; G Sutton for aiding multiangle light scattering experiments; and B Janssen, C Siebold and DI Stuart for critical reading of the manuscript. We are grateful to the staff of the Diamond Light Source for assistance with diffraction data collection. This research was funded by Cancer Research UK (CR-UK) and the UK Medical Research Council. ES is funded by an IEF Marie Curie fellowship, CHC was the recipient of a Wellcome Trust DPhil studentship, ARA is a UK Medical Research Council Career Development Award Fellow and EYJ is a Cancer Research UK Principal Research Fellow.

Author contributions: ES and CHC conducted crystallographic studies, SPR experiments and multiangle light scattering analyses. ES and PVP performed cellular assays and imaging. KH performed crystal mounting and aided X-ray data collection. All authors contributed to data analysis, discussion and preparation of the manuscript.

Conflict of interest

The authors declare that they have no conflict of interest.

References

Adams PD, Afonine PV, Bunkoczi G, Chen VB, Davis IW, Echols N, Headd JJ, Hung LW, Kapral GJ, Grosse-Kunstleve RW, McCoy AJ, Moriarty NW, Oeffner R, Read RJ, Richardson DC, Richardson JS, Terwilliger TC, Zwart PH (2010) PHENIX: a comprehensive Python-based system for macromolecular structure solution. *Acta Crystallogr D Biol Crystallogr* **66:** 213–221

Ango F, di Cristo G, Higashiyama H, Bennett V, Wu P, Huang ZJ (2004) Ankyrin-based subcellular gradient of neurofascin, an immunoglobulin family protein, directs GABAergic innervation at purkinje axon initial segment. *Cell* **119:** 257–272

Aoki-Suzuki M, Yamada K, Meerabux J, Iwayama-Shigeno Y, Ohba H, Iwamoto K, Takao H, Toyota T, Suto Y, Nakatani N, Dean B, Nishimura S, Seki K, Kato T, Itohara S, Nishikawa T, Yoshikawa T (2005) A family-based association study and gene expression analyses of netrin-G1 and -G2 genes in schizophrenia. *Biol Psychiatry* **57:** 382–393

Aricescu AR, Lu W, Jones EY (2006) A time- and cost-efficient system for high-level protein production in mammalian cells. *Acta Crystallogr D Biol Crystallogr* **62:** 1243–1250

Bella J, Hindle KL, McEwan PA, Lovell SC (2008) The leucine-rich repeat structure. *Cell Mol Life Sci* **65:** 2307–2333

Blanc E, Roversi P, Vonrhein C, Flensburg C, Lea SM, Bricogne G (2004) Refinement of severely incomplete structures with maximum likelihood in BUSTER-TNT. *Acta Crystallogr D Biol Crystallogr* **60:** 2210–2221

Borg I, Freude K, Kubart S, Hoffmann K, Menzel C, Laccone F, Firth H, Ferguson-Smith MA, Tommerup N, Ropers HH, Sargan D, Kalscheuer VM (2005) Disruption of Netrin G1 by a balanced chromosome translocation in a girl with Rett syndrome. *Eur J Hum Genet* **13:** 921–927

Chang VT, Crispin M, Aricescu AR, Harvey DJ, Nettleship JE, Fennelly JA, Yu C, Boles KS, Evans EJ, Stuart DI, Dwek RA, Jones EY, Owens RJ, Davis SJ (2007) Glycoprotein structural genomics: solving the glycosylation problem. *Structure* **15:** 267–273

Collaborative Computational Project 4 (1994) The CCP4 suite: programs for protein crystallography. *Acta Crystallogr D Biol Crystallogr* **50:** 760–763

Davis IW, Leaver-Fay A, Chen VB, Block JN, Kapral GJ, Wang X, Murray LW, Arendall III WB, Snoeyink J, Richardson JS, Richardson DC (2007) MolProbity: all-atom contacts and structure validation for proteins and nucleic acids. *Nucleic Acids Res* **35:** W375–W383

Eastwood SL, Harrison PJ (2008) Decreased mRNA expression of netrin-G1 and netrin-G2 in the temporal lobe in schizophrenia and bipolar disorder. *Neuropsychopharmacology* **33:** 933–945

Emsley P, Cowtan K (2004) Coot: model-building tools for molecular graphics. *Acta Crystallogr D Biol Crystallogr* **60:** 2126–2132

Fan QR, Hendrickson WA (2005) Structure of human follicle-stimulating hormone in complex with its receptor. *Nature* **433:** 269–277

Grueninger-Leitch F, D'Arcy A, D'Arcy B, Chene C (1996) Deglycosylation of proteins for crystallization using recombinant fusion protein glycosidases. *Protein Sci* **5:** 2617–2622

Hussain SA, Carafoli F, Hohenester E (2011) Determinants of laminin polymerization revealed by the structure of the alpha5 chain amino-terminal region. *EMBO Rep* **11:** 11

Kabsch W (1993) Automatic processing of rotation diffraction data from crystals of initially unknown symmetry and cell constants. *J Appl Crystallogr* **26:** 795–800

Kim S, Burette A, Chung HS, Kwon SK, Woo J, Lee HW, Kim K, Kim H, Weinberg RJ, Kim E (2006) NGL family PSD-95-interacting adhesion molecules regulate excitatory synapse formation. *Nat Neurosci* **9:** 1294–1301

Krissinel E, Henrick K (2007) Inference of macromolecular assemblies from crystalline state. *J Mol Biol* **372:** 774–797

Kwon SK, Woo J, Kim SY, Kim H, Kim E (2010) Trans-synaptic adhesions between netrin-G ligand-3 (NGL-3) and receptor tyrosine phosphatases LAR, protein-tyrosine phosphatase delta (PTPdelta), and PTPsigma via specific domains regulate excitatory synapse formation. *J Biol Chem* **285:** 13966–13978

Lai Wing Sun K, Correia JP, Kennedy TE (2011) Netrins: versatile extracellular cues with diverse functions. *Development* **138:** 2153–2169

Lawrence MC, Colman PM (1993) Shape complementarity at protein/protein interfaces. *J Mol Biol* **234:** 946–950

Lin JC, Ho WH, Gurney A, Rosenthal A (2003) The netrin-G1 ligand NGL-1 promotes the outgrowth of thalamocortical axons. *Nat Neurosci* **6:** 1270–1276

McCoy AJ, Grosse-Kunstleve RW, Adams PD, Winn MD, Storoni LC, Read RJ (2007) Phaser crystallographic software. *J Appl Crystallogr* **40:** 658–674

Meijers R, Puettmann-Holgado R, Skiniotis G, Liu JH, Walz T, Wang JH, Schmucker D (2007) Structural basis of Dscam isoform specificity. *Nature* **449:** 487–491

Mosyak L, Wood A, Dwyer B, Buddha M, Johnson M, Aulabaugh A, Zhong X, Presman E, Benard S, Kelleher K, Wilhelm J, Stahl ML, Kriz R, Gao Y, Cao Z, Ling HP, Pangalos MN, Walsh FS, Somers WS (2006) The structure of the Lingo-1 ectodomain, a module implicated in central nervous system repair inhibition. *J Biol Chem* **281:** 36378–36390

Murshudov GN, Vagin AA, Dodson EJ (1997) Refinement of macromolecular structures by the maximum-likelihood method. *Acta Crystallogr D Biol Crystallogr* **53:** 240–255

Nakashiba T, Ikeda T, Nishimura S, Tashiro K, Honjo T, Culotti JG, Itohara S (2000) Netrin-G1: a novel glycosyl phosphatidylinositol-linked mammalian netrin that is functionally divergent from classical netrins. *J Neurosci* **20:** 6540–6550

Nakashiba T, Nishimura S, Ikeda T, Itohara S (2002) Complementary expression and neurite outgrowth activity of netrin-G subfamily members. *Mech Dev* **111:** 47–60

Nishimura-Akiyoshi S, Niimi K, Nakashiba T, Itohara S (2007) Axonal netrin-Gs transneuronally determine lamina-specific subdendritic segments. *Proc Natl Acad Sci USA* **104:** 14801–14806

O'Callaghan CA, Byford MF, Wyer JR, Willcox BE, Jakobsen BK, McMichael AJ, Bell JI (1999) BirA enzyme: production and application in the study of membrane receptor-ligand interactions by site-specific biotinylation. *Anal Biochem* **266:** 9–15

Ohtsuki T, Horiuchi Y, Koga M, Ishiguro H, Inada T, Iwata N, Ozaki N, Ujike H, Watanabe Y, Someya T, Arinami T (2008) Association of polymorphisms in the haplotype block spanning the alternatively spliced exons of the NTNG1 gene at 1p13.3 with schizophrenia in Japanese populations. *Neurosci Lett* **435:** 194–197

Otwinowski Z, Minor W (1997) Processing of X-ray diffraction data collected in oscillation mode. *Methods Enzymol* **276:** 307–326

Pan Y, Liu G, Fang M, Shen L, Wang L, Han Y, Shen D, Wang X (2010) Abnormal expression of netrin-G2 in temporal lobe epilepsy neurons in humans and a rat model. *Exp Neurol* **224:** 340–346

Patel SD, Ciatto C, Chen CP, Bahna F, Rajebhosale M, Arkus N, Schieren I, Jessell TM, Honig B, Price SR, Shapiro L (2006) Type II cadherin ectodomain structures: implications for classical cadherin specificity. *Cell* **124:** 1255–1268

Ramelot TA, Raman S, Kuzin AP, Xiao R, Ma LC, Acton TB, Hunt JF, Montelione GT, Baker D, Kennedy MA (2009) Improving NMR protein structure quality by Rosetta refinement: a molecular replacement study. *Proteins* **75:** 147–167

Richardson JS (1981) The anatomy and taxonomy of protein structure. *Adv Protein Chem* **34:** 167–339

Sanes JR, Yamagata M (2009) Many paths to synaptic specificity. *Annu Rev Cell Dev Biol* **25:** 161–195

Sawaya MR, Wojtowicz WM, Andre I, Qian B, Wu W, Baker D, Eisenberg D, Zipursky SL (2008) A double S shape provides the structural basis for the extraordinary binding specificity of Dscam isoforms. *Cell* **134:** 1007–1018

Shi J, Blundell TL, Mizuguchi K (2001) FUGUE: sequence-structure homology recognition using environment-specific substitution tables and structure-dependent gap penalties. *J Mol Biol* **310:** 243–257

Suto F, Tsuboi M, Kamiya H, Mizuno H, Kiyama Y, Komai S, Shimizu M, Sanbo M, Yagi T, Hiromi Y, Chedotal A, Mitchell KJ, Manabe T, Fujisawa H (2007) Interactions between plexin-A2, plexin-A4, and semaphorin 6A control lamina-restricted projection of hippocampal mossy fibers. *Neuron* **53:** 535–547

Terwilliger TC, Grosse-Kunstleve RW, Afonine PV, Moriarty NW, Zwart PH, Hung LW, Read RJ, Adams PD (2008) Iterative model building, structure refinement and density modification with the PHENIX AutoBuild wizard. *Acta Crystallogr D Biol Crystallogr* **64:** 61–69

Tessier-Lavigne M, Kolodkin AL (2011) *Neuronal Guidance: The Biology of Brain Wiring*. New York: Cold Spring Harbor Laboratory Press

Walter TS, Diprose JM, Mayo CJ, Siebold C, Pickford MG, Carter L, Sutton GC, Berrow NS, Brown J, Berry IM, Stewart-Jones GB, Grimes JM, Stammers DK, Esnouf RM, Jones EY, Owens RJ, Stuart DI, Harlos K (2005) A procedure for setting up high-throughput nanolitre crystallization experiments. Crystallization workflow for initial screening, automated storage, imaging and optimization. *Acta Crystallogr D Biol Crystallogr* **61:** 651–657

Williams ME, de Wit J, Ghosh A (2010) Molecular mechanisms of synaptic specificity in developing neural circuits. *Neuron* **68:** 9–18

Winter G (2010) xia2: an expert system for macromolecular crystallography data reduction. *J Appl Cryst* **43:** 186–190

Woo J, Kwon SK, Choi S, Kim S, Lee JR, Dunah AW, Sheng M, Kim E (2009a) Trans-synaptic adhesion between NGL-3 and LAR regulates the formation of excitatory synapses. *Nat Neurosci* **12:** 428–437

Woo J, Kwon SK, Kim E (2009b) The NGL family of leucine-rich repeat-containing synaptic adhesion molecules. *Mol Cell Neurosci* **42:** 1–10

Yin Y, Miner JH, Sanes JR (2002) Laminets: laminin- and netrin-related genes expressed in distinct neuronal subsets. *Mol Cell Neurosci* **19:** 344–358

Zhang W, Rajan I, Savelieva KV, Wang CY, Vogel P, Kelly M, Xu N, Hasson B, Jarman W, Lanthorn TH (2008) Netrin-G2 and netrin-G2 ligand are both required for normal auditory responsiveness. *Genes Brain Behav* **7:** 385–392

